Thermochimica Acta 512 (2011) 13–21

Contents lists available at ScienceDirect

Thermochimica Acta

journal homepage: www.elsevier.com/locate/tca

Thermally induced transformations of calcium carbonate polymorphs precipitated selectively in ethanol/water solutions

Nobuyoshi Koga*, Yuko Yamane, Tomoyasu Kimura

Chemistry Laboratory, Department of Science Education, Graduate School of Education, Hiroshima University, 1-1-1 Kagamiyama, Higashi-Hiroshima 739-8524, Japan

ARTICLE INFO

Article history:
Received 1 June 2010
Received in revised form 15 August 2010
Accepted 19 August 2010
Available online 26 August 2010

Keywords:
Calcium carbonate polymorphs
Amorphous calcium carbonate
Vaterite
Calcite
Thermal behavior

ABSTRACT

For the precipitation of calcium carbonate polymorphs in ethanol/water solutions of calcium chloride by the diffusion of the gases produced by sublimation–decomposition of solid ammonium carbonate, polymorph selection and morphology control of the precipitates were demonstrated by the effect of ethanol/water ratio in the mother liquor. The precipitated phases change systematically from gel-like aggregates of hydrated amorphous calcium carbonate in the absolute ethanol solution to well-shaped rhombohedral particles of calcite in the absolute aqueous solution via almost pure phase of vaterite with dendrite structure in 75%-ethanol/25%-aqueous and 50%-ethanol/50%-aqueous solutions. On heating the precipitated sample in flowing dry nitrogen, all the samples transformed to calcite before the thermal decomposition, where the thermal decomposition temperature shifts to higher temperatures with increasing the water content in the mother liquor due to the systematic increase in the particle size of calcite. Accordingly, the present method of controlled precipitation of calcium carbonate polymorphs is also useful to control the particle size and reactivity of calcite produced by heating the precipitates. Selecting vaterite with dendrite structure from the present series of precipitated samples, the structural phase transition to calcite was characterized as the three-dimensional growth of rhombohedral particles of calcite with the enthalpy change $\Delta H = -2.8 \pm 0.1\ \mathrm{kJ\,mol^{-1}}$ and the apparent activation energy $E_a = 289.9 \pm 5.8\ \mathrm{kJ\,mol^{-1}}$.

1. Introduction

Selective synthesis and morphology control of calcium carbonate polymorphs (CCPs) including amorphous calcium carbonate (ACC) through precipitation reactions from mother liquors have long been studied by many workers due to their various industrial applications such as additives and fillers in medicine, foods, plastics, printing ink, etc. It is well known that these CCPs are the typical biominerals that exhibit various specialized morphologies and architectures [1,2]. Learning after biomineralization of calcium carbonate in living organisms [3–10], recent researches on the formation processes of CCPs have been concentrated to control the nucleation of a favored phase, crystal growth to a selected direction, self-assemblage or agglomeration of nanoparticles, hybridization with polymer, etc. in a highly systematic way by regulating various reaction conditions at the respective reaction steps [11,12]. Interactions of inorganic ions with organic (macro)molecules have been applied to control the respective reaction steps, resulting in successful polymorph selection, morphology control, and composite generation by variously designed biomimetic mineralization processes [13]. In such biomimetic mineralization of CCPs, the roles of ACC to transform a selected polymorph with a specialized morphology and architecture are special interest [14]. Variously oriented material synthesis of CCPs such as nano-sized functional materials [15–18], inorganic–organic hybrid materials [19–21], thin films [22–27], and so on were examined through ACC precursor pathways, together with examinations on the preparation and stabilization methods of ACC [28–34] and on the physico-chemical properties of ACC such as structural and thermal properties [35,36].

At the same time, CCPs are also the precursors of many functional ceramics so that thermally induced structural phase transitions of CCPs [37–48], i.e., the transformations from metastable phases of vaterite and alagonite to stable phase of calcite, and thermal decomposition of calcite [49–54] have been subjected to thermodynamic and kinetic studies for gathering fundamental information on applying for the ceramic processing. In such reactions in the solid-state, the physico-chemical mechanism of the reaction and the properties of product solids are influenced largely by the morphology of the reactant solid [55,56]. In this point, it is expected that recent advancements of polymorph selection and morphology control of CCPs precipitations enable us to characterize the thermodynamics and kinetics of those solid-state transformations of the reactant solids with the rigorously controlled and/or highly specialized morphologies, which is useful for controlling

* Corresponding author. Tel.: +81 82 424 7092; fax: +81 82 424 7092.
E-mail address: nkoga@hiroshima-u.ac.jp (N. Koga).

0040-6031/$ – see front matter © 2010 Elsevier B.V. All rights reserved.
doi:10.1016/j.tca.2010.08.016

the physico-geometry of the reaction processes and the assembled structure of the products in an advanced ceramic processing.

The present study is aimed to interlink those researches on calcium carbonate orientated differently, expecting the compensative integration of those studies by focusing on the thermal behavior of the systematically controlled CCPs. A precipitation reaction in a calcium chloride solution by diffusion of the gases produced by sublimation–decomposition of solid ammonium carbonate was selected for the preparation technique of CCPs. When using aqueous solution of calcium chloride, well-shaped rhombohedral particles of calcite are obtained [22,57]. By changing the solvent to ethanol, unusually stable gel-like precipitates of hydrated ACC are obtained under the conditions otherwise identical with the formation of calcite in the aqueous solution [31]. As has been utilized for the polymorph selection and morphology control in the other preparation techniques of CCPs in calcium chloride solutions such as CO_2 bubbling, urea decomposition, and diffusion of sublimated–decomposed $(NH_4)_2CO_3$ [58–60], changes in the polymorphs and morphologies of the precipitates from hydrated ACC in ethanol solution to calcite in aqueous solution were examined by changing systematically the ethanol/water composition of the solvent. From the viewpoints of solid-state reaction, thermal behaviors of the as-precipitated samples were investigated and characterized by considering the polymorph composition and the morphology. The structural phase transition of vaterite with a dendritic branching structure, precipitated in the present study from an ethanol/water solution, to calcite was subjected to the kinetic study for demonstrating the dependence of the apparent kinetics of the transformation and morphology of the product calcite on the morphological characteristics of the vaterite particles.

2. Experimental

2.1. Sample preparation

An ethanol solution of 0.01 mol dm^{-3} $CaCl_2$ was prepared using chemical reagents of anhydrous $CaCl_2$ (special grade ≥95.0%, Wako Chem.) and ethanol (special grade ≥99.5%, Sigma–Aldrich Japan). An aqueous solution of the same concentration was prepared by dissolving chemical regent of $CaCl_2$ dihydrate (special grade ≥99.0%, Sigma–Aldrich Japan) into deionized–distilled water. The ethanol and aqueous solutions were mixed in various volume ratios. About 10 g of solid $(NH_4)_2CO_3$ (special grade, ≥30% NH_3 basis, Sigma–Aldrich Japan) was spread in a cylindrical separable flask (500 cm^3). A beaker (200 cm^3) with 200 cm^3 of the mixed solution was placed in the flask, which was sealed up using a lid (200 cm^3) for the separable flask. The closed reaction vessel was left at a controlled ambient temperature of 293 K for 24 h. Precipitates obtained were filtered and washed with ethanol and/or water. The filtrate was dried in a vacuum desiccator for 24 h and stored in a refrigerator at 278 K. The samples obtained from different mixed solutions were labeled using the volume-% of the ethanol (ET) and aqueous (AQ) solutions such as ET75AQ25 for the mixed solution with 75%-ethanol solution/25%-aqueous solutions.

2.2. Measurements

The crystalline phase of the as-precipitated samples was characterized by powder X-ray diffractometry (XRD) using a RINT2200V (Rigaku Co.; monochrome Cu-K_α, 40 kV, 20 mA, 4° min^{-1}). After diluting the samples with KBr, Fourier transform infrared spectra were recorded with a FT-IR8400 M (Shimadzu Co.) by the diffuse reflectance method. The morphologies of the samples were observed using a scanning electron microscope (SEM, S-2460N, Hitachi Co.) after coating the samples with Au evaporation.

Using a TGD9600 (ULVAC), simultaneous measurements of thermogravimetry and differential thermal analysis (TG–DTA) were performed by heating the samples of 10.0 mg, weighed into a platinum cell (5 mm in diameter, 5 mm in height), at 10 K min^{-1} under flowing N_2 (100 cm^3 min^{-1}). Phase changes during heating the samples were traced using the above XRD instrument by equipping with a programmable heating chamber (PTC-20A, Rigaku Co.). By heating the samples, press-fitted to a platinum plate, at 10 K min^{-1} under flowing N_2 (100 cm^3 min^{-1}), XRD measurements were started at various temperatures where the sample temperature was kept constant during the diffraction measurement for 15 min. The samples heated to some selected temperature in the above TG–DTA were subjected to FT-IR measurement and SEM observation, in order to identify the thermally induced physicochemical events. The phase transition from vaterite to calcite observed for some samples was traced by differential scanning calorimetry (DSC) using a DSC8270 (Rigaku Co.). The DSC measurements were carried out using 10.0 mg of sample, weighed into a platinum cell (5 mm in diameter, 3 mm in height) and covered up with a platinum lid, at various heating rates in flowing N_2 (50 cm^3 min^{-1}), where 10.0 mg of α-Al_2O_3 were used as the reference material.

3. Results and discussion

3.1. Characterization of precipitates

By exposing the series ethanol/water solutions of $CaCl_2$ to the gases produced by sublimation–decomposition of solid $(NH_4)_2CO_3$, i.e., NH_3, CO_2 and water vapor, for 24 h in a closed vessel, precipitation reactions took place irrespective of the mother liquors with different ethanol/water compositions. Appearance of the precipitates in the respective mother liquors varied systematically from colloidal precipitates of ET100AQ0 to well-crystallized precipitates of ET0AQ100.

Fig. 1 compares typical XRD patterns of the as-precipitated samples in the respective mother liquors. As has been reported in our previous paper [36], ET100AQ0 indicates a halo centered at around 27.5° without any distinguished diffraction peaks. With increasing the ratio of water in the mother liquor to 5%, i.e., ET95AQ5, the diffraction peaks ascribed to vaterite phase appear. The diffraction peaks grow with increasing the water content in the mother liquor up to 50%, i.e., ET50AQ50. Further increase in the water content results in the appearance of the diffraction peaks of calcite as is seen for ET25AQ75 identified as the mixed phases of vaterite and calcite. For ET0AQ100, the XRD pattern corresponds almost to that of calcite with the detectable trace of vaterite. Such changes of the precipitated phases are clearly seen by the IR absorption due to internal ν_4 mode of CO_3^{2-} as shown in Fig. 2 [61]. For the amorphous precipitate of ET100AQ0, no distinguished absorption peak due to $\nu_4(CO_3^{2-})$ is observed. With increasing the water content in the mother liquor, absorption peak at 745 cm^{-1} corresponding to $\nu_4(CO_3^{2-})$ of vaterite appears and grows. The absorption peak at 712 cm^{-1}, the ν_4 mode of CO_3^{2-} for calcite appears for ET50AQ50 and grows with further increase in the water content accompanying with the attenuation of the absorption peak at 745 cm^{-1}.

Fig. 3 compares the SEM images of the as-precipitated samples from the different mother liquors. The amorphous phase of ET100AQ0 looks like a gel aggregate, Fig. 3(a). Vaterite phase precipitated from the mother liquors with low water contents, i.e., ET95AQ5 and ET90AQ10, consisted of spherical particles with a fairly monodispersive distribution, Fig. 3(b) and (c). By increasing the water contents in the mother liquors, morphology of vaterite precipitates changes to dendritic branching structure constructed with spindle-shaped aggregates of nanoparticles as is

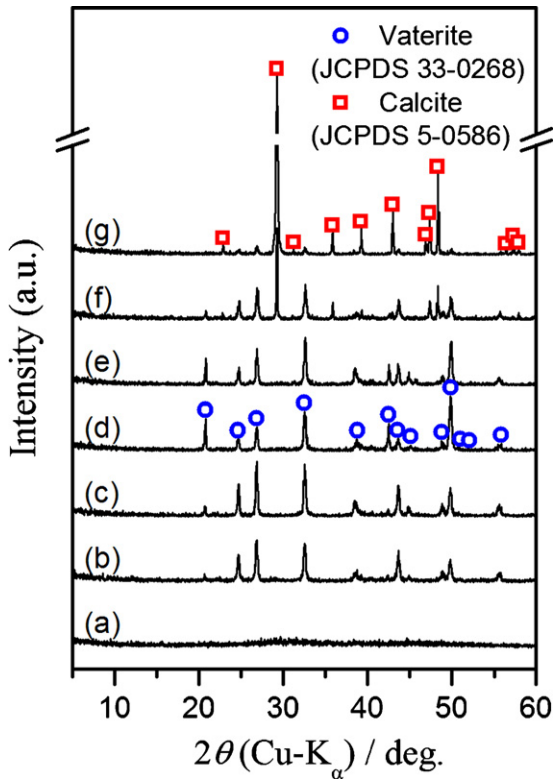

Fig. 1. Typical XRD patterns of the as-precipitated samples. (a) ET100AQ0, (b) ET95AQ5, (c) ET90AQ10, (d) ET75AQ25, (e) ET50AQ50, (f) ET25AQ75, and (g) ET0AQ100.

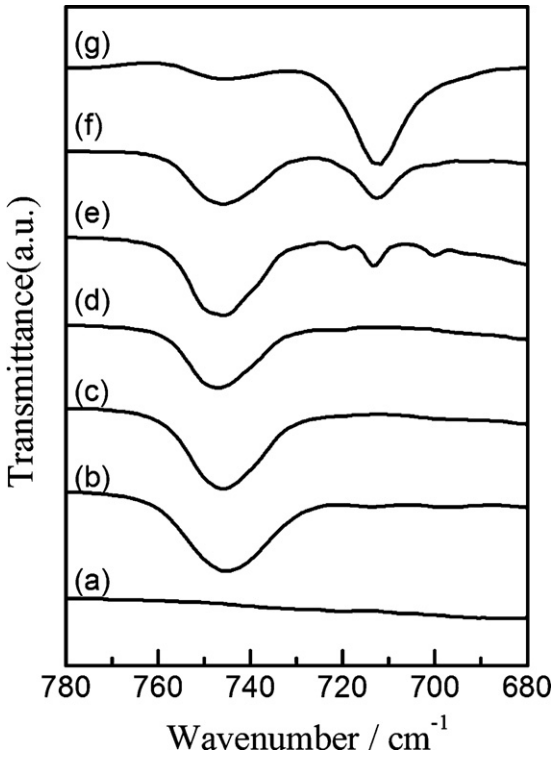

Fig. 2. Typical FT-IR spectra of the as-precipitated samples. (a) ET100AQ0, (b) ET95AQ5, (c) ET90AQ10, (d) ET75AQ25, (e) ET50AQ50, (f) ET25AQ75, and (g) ET0AQ100.

shown in Fig. 3(d) and (e) for ET75AQ25 and ET50AQ50, respectively.

The observed variation in the morphology of vaterite precipitates followed the same trend with the crystallization of vaterite from surfactant-stabilized amorphous calcium carbonate (ACC) induced by the addition of water reported by Li and Mann [15], where a range of organized hybrid surfactant–vaterite nanostructures was produced. It was reported [15] that, when the low amount of water was added to alkylbenzensulfonate-coated ACC nanoparticles in water-in-isooctane sodium bis(2-ethlhexyle)sulfosuccinate microemulsions, monodisperse spherical aggregates of densely packed 5 nm diameter surfactant-coated vaterite nanoparticles were produced as is the present case of ET95AQ5 and ET90AQ10. Decreasing the extent of coupling at the surface–inorganic interface by the addition of higher amount of water, the morphology of vaterite changed to anisotropic nanostructures of spindle-shaped aggregates of 18 nm sized vaterite nanoparticles as was observed for ET75AQ25 and ET50AQ50 in the present study. It is known that the hydrated ACC is stabilized in ethanol being inhibited the solution mediated phase transformation to vaterite or calcite [31]. It is expected that the present variation of vaterite morphology depending on the ethanol/water composition in the mother liquor results from the variation of the stability of ethanol solvated ACC nanoparticles with the extent of coupling at the surface-in-ethanol interface.

By further increase in the water contents in the mother liquor, rhombohedral particles of calcite with rough surfaces appear for ET25AQ75, mixed in with spindle-shaped aggregates of vaterite, see Fig. 3(f). Well-shaped rhombohedral particles of calcite with smooth surfaces become the major component of ET0AQ100 as can be seen in Fig. 3(g). In the same reaction scheme to the present study, the compositional changes of the precipitated CCPs in the limited region of ethanol <50% have been examined by Dickinson and McGrath [60]. Although the mixed phases of calcite and vaterite have been obtained in the study as in the present study, the systematic change of the CCPs composition with the ethanol/water ratio of the mother liquor was not observed.

In comparison with the previous studies on the CCPs fabrication in the same reaction scheme, the present samples are characteristic in the appearances of nearly pure phases of hydrated ACC, vaterite, and calcite with varying ethanol/water ratio of the mother liquor. This observation is valuable both for the further detailed examination of the chemistry of the mineralization process and for the systematic evaluation of the thermal behavior of the series of the samples, where the latter is the present scope of the study.

3.2. Thermal behaviors

Fig. 4 compares typical TG–DTA curves of the as-precipitated samples. ET100AQ0 indicates initial mass-loss of $22.0 \pm 0.7\%$ accompanied by a wide endothermic peak during heating from room temperature to 600 K. The mass-loss process is ascribed to the thermal dehydration of hydrated ACC [36,46]. Slight but detectable mass-loss in the same temperature range is observed for ET95AQ5 and ET90AQ10, indicating that the hydrated ACC is incorporated in these samples as the secondary phase in addition to vaterite phase detected by XRD. A distinguished exothermic peak observed at the end of the thermal dehydration of ET100AQ0 is due to the crystallization of anhydrous ACC to calcite phase [36,46]. The corresponding exothermic peaks are observed for ET95AQ5 and ET90AQ10, where the peak temperature shifts higher temperature and the peak area decreases with increasing the water content in the mother liquor. No trace of the exothermic peak can be detected for the other samples.

The second exothermic peak observed for ET100AQ0 at around 800–900 K has been characterized as the crystal growth of poorly crystalline calcite phase with developing a rightly stacking struc-

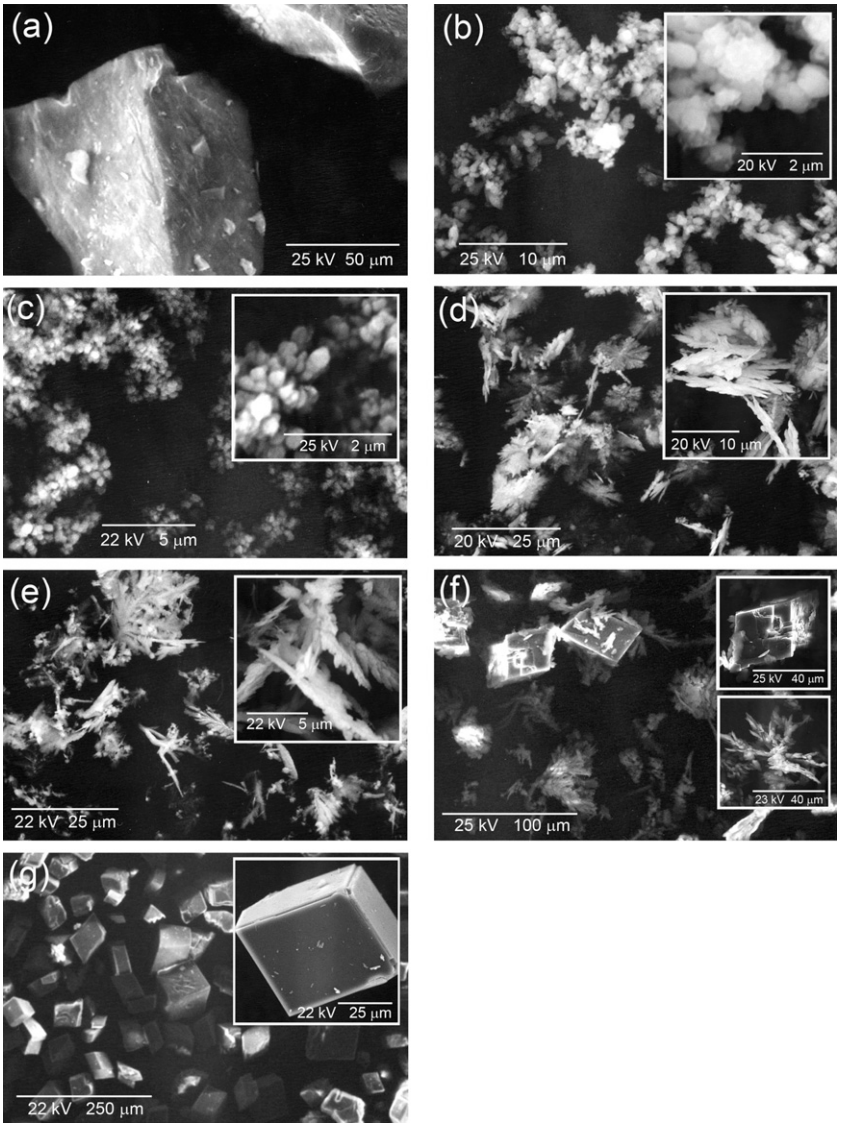

Fig. 3. Typical SEM images of the as-precipitated samples. (a) ET100AQ0, (b) ET95AQ5, (c) ET90AQ10, (d) ET75AQ25, (e) ET50AQ50, (f) ET25AQ75, and (g) ET0AQ100.

ture [36] as shown in Fig. 5, where the minor phase of vaterite produced during the crystallization of anhydrous ACC also transforms to calcite. It has also been revealed [36] that the enthalpy change ΔH for the second exothermic peak of ET100AQ0 increases systematically with increasing the heating rate applied, i.e., $-6.6\,\mathrm{kJ\,(mol\,CaCO_3)^{-1}}$ at $2\,\mathrm{K\,min^{-1}}$ to $-12.2\,\mathrm{kJ\,(mol\,CaCO_3)^{-1}}$ at $10\,\mathrm{K\,min^{-1}}$, indicating the gradual proceeding of crystal growth of the poorly crystalline calcite between the first and second exothermic peaks.

In the same temperature region with the second exothermic peak of ET100AQ0, ET75AQ25, characterized as almost single phase of vaterite, also indicates an exothermic peak. By DSC measurements, it was confirmed that the corresponding exothermic peak area is invariant at different heating rates with the mean value of $\Delta H = -2.8 \pm 0.1\,\mathrm{kJ\,(mol\,CaCO_3)^{-1}}$. The ΔH value observed for the exothermic peak of ET75AQ25 is fairly in good agreement with the values reported for the thermally induced transformation of vaterite to calcite, i.e., -3.1 ± 0.1 [45], -3.4 [42], and $-3.5\,\mathrm{kJ\,(mol\,CaCO_3)^{-1}}$ [37]. Fig. 6 shows changes of powder XRD patterns during stepwise heating of ET75AQ25. The original vaterite phase transforms to calcite at the temperature corresponding to the DTA exothermic peak. The transformation is clearly seen by comparing the IR absorption ascribed to ν_4 mode of CO_3^{2-} for the samples heated to just before and after the exothermic peak as was shown in Fig. 7. Fig. 8 compares typical SEM images of the samples, ET75AQ25, heated to just before and after the transformation. The dendritic branching structure of vaterite changes to the aggregates of well-shaped rhombohedral particles. The exothermic peak of the transformation is observed up to ET25AQ75 by lowering the transformation temperature and decreasing the peak area with increasing the water contents in the mother liquor. In spite of the detectable trace of vaterite phase in XRD, ET0AQ100 did not indicate the corresponding exothermic peak.

Irrespective of the samples, the mass-loss processes in the temperature region higher than 850 K are thus due to the thermal decomposition of calcite. The observed mass-loss values for the respective samples are all in good agreement with 44.0% calculated by assuming: $CaCO_3 \rightarrow CaO + CO_2$. On the other hand, the temperature region and shape of the TG curve vary systematically with the ethanol/water composition of the mother liquor. It is well known that the thermal decomposition process of calcite vary sensitively with the characteristics of the sample particles and the reaction conditions [51]. Among others, the physico-geometric kinetic behavior is influenced largely by the particle size and its dis-

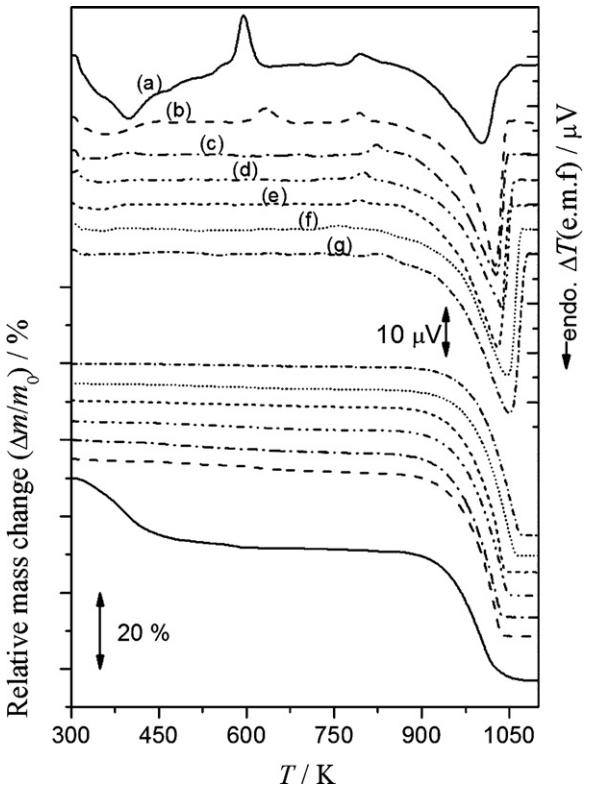

Fig. 4. Typical TG–DTA curves at 10 K min^{-1} under flowing N_2 (100 cm^3 min^{-1}) of the as-precipitated samples. (a) ET100AQ0, (b) ET95AQ5, (c) ET90AQ10, (d) ET75AQ25, (e) ET50AQ50, (f) ET25AQ75, and (g) ET0AQ100.

tribution [62], partial pressure of CO_2 in reaction atmosphere [53], mass-transfer phenomena of evolved CO_2 [54], and so on.

By considering such characteristics of the thermal decomposition process, the variations of TG curves for the present series of samples can be interpreted as follows. The thermal decomposition of calcite phase produced from ET100AQ0 by the crystallization of anhydrous ACC indicates a sigmoid TG curve over the temperature region wider than those of the others. Because the calcite phase is aggregates of calcite particles with the stacking structure, see Fig. 5,

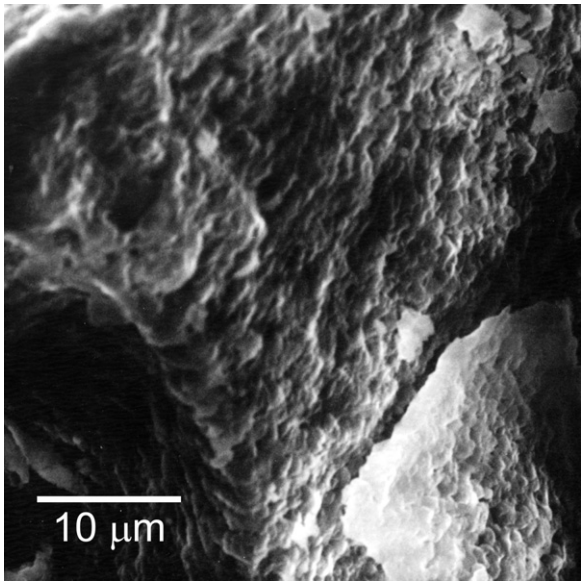

Fig. 5. A Typical SEM image of ET100AQ0 heated to 853 K.

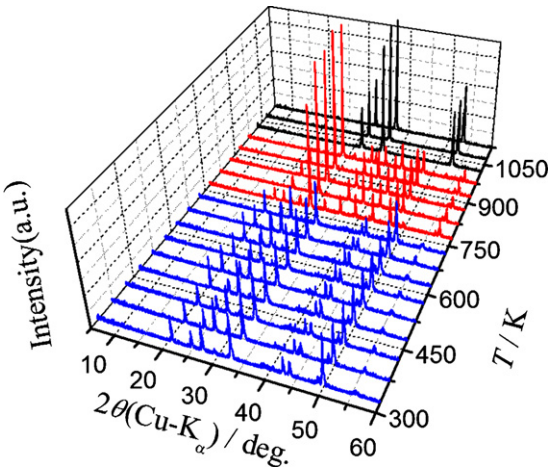

Fig. 6. Changes of XRD patterns of ET75AQ25 during stepwise heating.

the thermal decomposition initiates at surface of the aggregates and subsequently proceeds inwards. The reaction of calcite particle in the internal of aggregates seems to be restrained by the increase in the partial pressure of CO_2 evolved by the reaction itself. It is expected that the characteristics of the TG curve for the thermal decomposition of calcite in ET100AQ0 result from such physico-geometric factors of the reaction as the aggregates. For the series of samples from ET95AQ5 to ET0AQ100, the TG curves of the thermal decomposition indicate the similar monotonous acceleration, which shift systematically to the higher temperature region with increasing the water content in the mother liquor. As can be seen in Figs. 3(g) and 8(b), the reactants of the thermal decomposition processes of the respective samples are the rhombohedral calcite particles with different particle sizes. Because the reactions of the respective particles are described geometrically by nucleation-growth at the particle surfaces and subsequent advancement of as-produced reaction interfaces inwards, a systematic increase in the particles size of calcite can be the major factor of the shift of reaction temperatures to higher temperatures. The above findings imply that fabrication of CCPs by the present method makes it possible to control not only the precipitated phase and morphology of CCPs, but also the size and morphology of calcite particles produced during heating those precipitated samples.

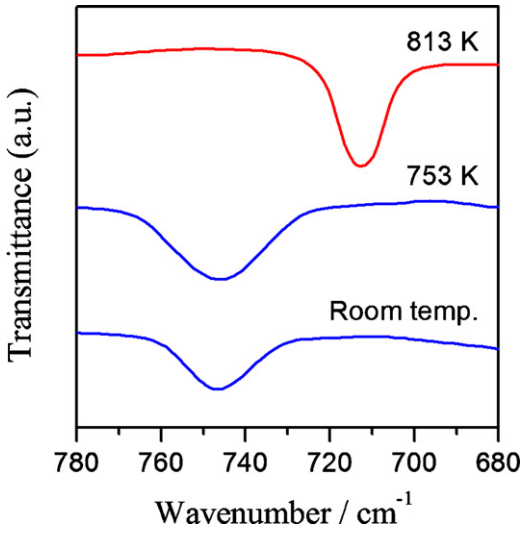

Fig. 7. Change of FT-IR spectra of ET75AQ25 during the exothermic DTA peak.

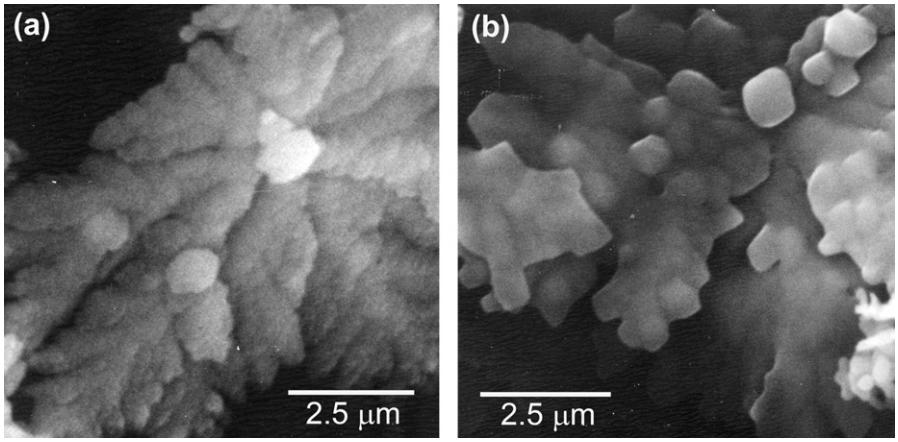

Fig. 8. Changes of SEM images during the exothermic DTA peak for ET75AQ25: (a) 753 K; (b) 813 K.

3.3. Kinetics of thermally induced transformation of vaterite to calcite

Phase transitions from anhydrous ACC and vaterite to calcite are observed on heating the present samples. We have reported that the kinetic behaviors of thermally induced crystallization of anhydrous ACC to calcite change largely influenced by the preparation conditions of precursor, i.e., hydrated ACC [36,46]. Changes in number of possible nucleation sites and in the structure and/or strength of gel-like aggregates of anhydrous ACC have been suggested as the possible causes of the variation of physico-geometric mechanisms of the nucleation and growth processes. The thermally induced structural transition from vaterite to calcite has also been subjected to the kinetic studies by many workers [38–42,44,45]. Although a kinetic behavior of random nucleation and growth type has been observed for the transformation, the reported kinetic parameters are distributing largely among the workers and depending on the preparation conditions of vaterite. Being accepted generally for the kinetic analysis of the solid-state reactions [55,56], it has been suggested [42] that experimental findings on the morphology of the reactant, vaterite, and its changes during the transformation are useful for interpreting the kinetic results evaluated empirically from the kinetic rate data such as thermoanalytical curves.

As was seen in Fig. 3(d) and (e), the morphology of the vaterite phase prepared in the present study, i.e., ET75AQ25 and ET50AQ50, was characterized as dendritic branching structure constructed with spindle-like aggregates of nanoparticles. The construction is maintained during heating the sample to just before the phase transition, see Fig. 8(a). By the phase transition to calcite, rhombohedral particles of calcite are produced on the original dendritic branching structure. From such morphological observations, three-dimensional growth of calcite particles from possible nucleation sites and/or pre-existing nuclei can be estimated as the physico-geometric mechanism of the structural phase transition.

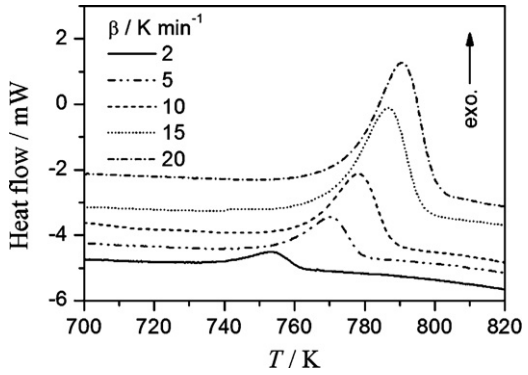

Fig. 9. Typical DSC curves for the transformation from vaterite (ET75AQ25) to calcite at different β.

Based on the above, the formal kinetic analysis for the phase transition from vaterite (ET75AQ25) to calcite was carried out by means of DSC measurements at different β. Fig. 9 shows the DSC curves for the structural phase transition at different β. Although two divided peak tops of DSC curve for the vaterite transition have been reported by Nassrallah-Aboukaïs et al. [48], the present sample indicated, irrespective of β applied, smooth DSC curves with the distinguished single peak top. By using the DSC curves as the series of kinetic rate data, the apparent activation energies, E_a, at different fractional conversion, α, were evaluated by Friedman method [63] based on the following equation.

$$\ln \frac{d\alpha}{dt} = \ln[Af(\alpha)] - \frac{E_a}{RT} \quad (1)$$

where A and $f(\alpha)$ are the pre-exponential factor of Arrhenius equation and kinetic model function in differential form, respectively. Fig. 10 represents the results of the Friedman plots of $\ln(d\alpha/dt)$ against T^{-1} at various selected α. At a selected α, all the data points recorded at different β line up on a straight line, see Fig. 10(a). At the same time, slopes of the plots, $-E_a/R$, do not change practically irrespective of the selected α, so that the values of E_a calculated from the slopes are constant over wide range of α with $289.9 \pm 5.8\ \mathrm{kJ\,mol^{-1}}$ averaged over $0.1 \leq \alpha \leq 0.9$, see Fig. 10(b). The results indicate that, within the reaction conditions of the present series of kinetic rate data, the kinetic process under investigation satisfies the isoconversional kinetic relationship based on the Arrhenius type temperature dependence and the relationship does not change during the course of reaction, that are the prerequisites of the kinetic analysis using Eq. (1).

For such an ideal kinetic process, three kinds of experimental master plots can be drawn by extrapolating the measured rate data to infinite temperature [64–66]. Fig. 11 represents such experimental master plots, where the error bars indicate the standard deviation of the respective y values calculated from the respective kinetic rate data recorded at different β. The experimental master plot in differential form can be drawn by extrapolating the measured conversion rate $(d\alpha/dt)$ to infinite temperature according to the following equation [64–67].

$$\left(\frac{d\alpha}{d\theta}\right)_\alpha = \left(\frac{d\alpha}{dt}\right)_\alpha \exp\left(\frac{E_a}{RT}\right) \quad \text{with} \quad \theta = \int_0^t \exp\left(-\frac{E_a}{RT}\right) dt \quad (2)$$

where θ is Ozawa's generalized time [68,69] denoting the reaction time at infinite temperature. The experimental master plot of $d\alpha/d\theta$

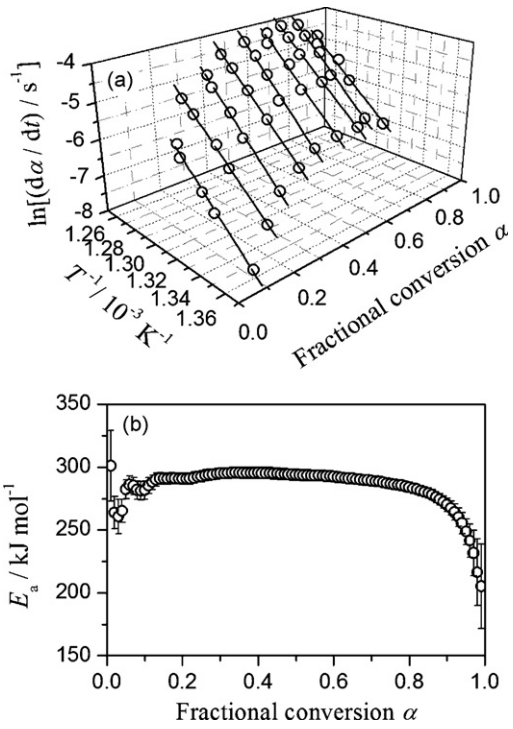

Fig. 10. Evaluation of apparent activation energy. (a) Friedman plots at different α and (b) the values of E_a at various α.

against α is further correlated with $f(\alpha)$ by the simple equation [64–67].

$$\left(\frac{d\alpha}{d\theta}\right) = Af(\alpha) \tag{3}$$

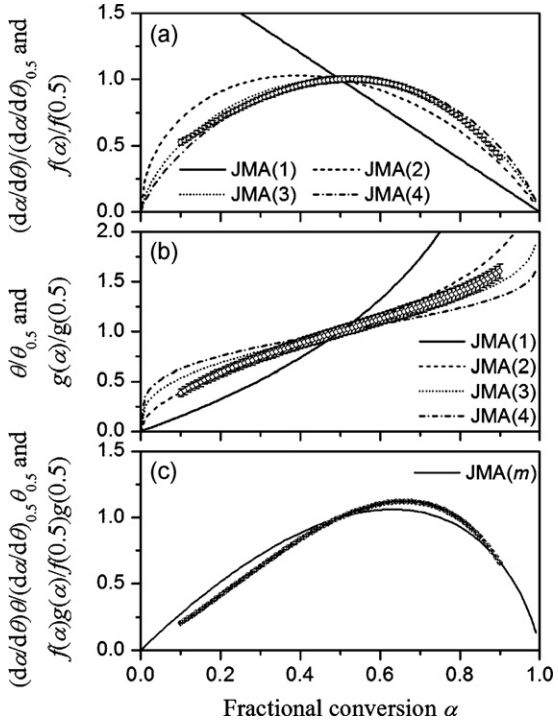

Fig. 11. Comparisons of the experimental master plots at infinite temperature with the theoretical curves drawn by assuming the kinetic model functions of JMA(m) type (a) in differential form, (b) in integral form, and (c) in multiplied form.

Fig. 11(a) shows the normalized plot of $(d\alpha/d\theta)/(d\alpha/d\theta)_{0.5}$ against α drawn by assuming the constant E_a of 289.9 kJ mol^{-1} ($0.1 \le \alpha \le 0.9$) for the transition of vaterite (ET75AQ25), which has the maximum $d\alpha/d\theta$ at $\alpha = 0.52$ and indicates the kinetic obedience to one of the nucleation-growth type reactions [70,71]. Through comparisons with the theoretical curves for the typical nucleation-growth type model, i.e., Johnson–Mehl–Avrami–Erofeyev–Kolgomorov model JMA(m) [72,73]: $f(\alpha) = m(1-\alpha)[-\ln(1-\alpha)]^{1-1/m}$, it is apparent that the experimental master plot is nearly corresponding to JMA(3).

Similarly, the experimental master plot in integral form, θ against α, is also useful to distinguish the appropriate kinetic model function. The value of θ at a selected α is evaluated from the kinetic rate data at a constant heating rate β according to the equation [64–69].

$$\theta = \frac{1}{\beta}\int_0^T \exp\left(-\frac{E_a}{RT}\right) dT = \frac{E_a}{\beta R}\int_x^\infty \frac{\exp(-x)}{x^2} dx \cong \frac{E_a}{\beta R}\frac{\exp(-x)}{x^2}\pi(x)$$

with

$$x = \frac{E_a}{RT} \quad \text{and} \quad \pi(x) = \frac{x^3 + 18x^2 + 86x + 96}{x^4 + 20x^3 + 120x^2 + 240x + 120} \tag{4}$$

where $\pi(x)$ is the fourth rational approximation of exponential integral [74,75]. The experimental master plot in integral form can be correlated to the kinetic model function in integral form $g(\alpha)$ by the equation obtained by integrating Eq. (3) [64–69].

$$g(\alpha) = \int_0^\alpha \frac{d\alpha}{f(\alpha)} = A\int_0^\theta d\theta = A\theta \tag{5}$$

As can be seen in Fig. 11(b), comparison of the experimental master plot in integral form with the theoretical curve of JMA(m) model, $g(\alpha) = [-\ln(1-\alpha)]^{1/m}$, also supports a fairly good correspondence to JMA(3).

By multiplying these experimental master plots in differential and integral forms, we obtain an alternative master plot of $(d\alpha/d\theta)\theta$ against α [65,66,69,70]. The multiplied master plot can be correlated directly to the kinetic model function by

$$\left(\frac{d\alpha}{d\theta}\right)\theta = f(\alpha)g(\alpha) \tag{6}$$

As for JMA(m) model, the theoretical curve of the multiplied function $f(\alpha)g(\alpha) = m(1-\alpha)[-\ln(1-\alpha)]$ against α is independent of the kinetic exponent m after normalizing at $\alpha = 0.5$ [67,70,71], so that comparison with the normalized experimental master plot in multiplied form, $(d\alpha/d\theta)\theta/(d\alpha/d\theta)_{0.5}\theta_{0.5}$ against α makes it possible to evaluate critically the kinetic correspondence of the process under investigation to JMA(m) model. The present process is nearly described by JMA(m) as was observed above, but the slight difference from the ideal JMA(m) model can be detected in Fig. 11(c), being characterized by the deviation of the α value at the maximum, i.e., $\alpha = 0.63$ for JMA(m) and $\alpha = 0.66$ for the present process.

For the final optimizations of the most appropriate kinetic model function and the value of A, empirical functions of Sestak–Berggren model [76], SB(m, n, p): $f(\alpha) = \alpha^m(1-\alpha)^n[-\ln(1-\alpha)]^p$, which fits to various physico-geometric types of reaction and those deviated cases [77,78], was employed by considering the possible deviations of the kinetic process from the idealized kinetic model, together with JMA(m) with non-integral kinetic exponent. Based on Eq. (2), the optimization was performed by fitting the experimental master plot of $d\alpha/d\theta$ against α with these kinetic model functions through the nonlinear least square fitting [79,80] by the Levenberg–Marquardt optimization algorithm. Fig. 12 shows the results of model fitting. The experimental master plot is nearly perfectly fitted by SB(−4.10, 2.55, 4.67). The fitting curve by JMA(3.34)

Table 1
Kinetic results for the thermally induced phase transition from vaterite (ET75AQ25) to calcite.

E_a [a] (kJ mol^{-1})	Kinetic model	Kinetic exponents	A (s^{-1})	γ^2 [b]
289.9 ± 5.8	JMA(m)	m = 3.34 ± 0.04	(2.03 ± 0.02) × 10^{17}	0.9880
	SB(m, n, p)	m = −4.10 ± 0.19	(4.97 ± 0.07) × 10^{17}	0.9987
		n = 2.55 ± 0.07		
		p = 4.67 ± 0.18		

[a] Averaged over $0.1 \leq \alpha \leq 0.9$.
[b] Correlation coefficient of the nonlinear regression analysis.

is very close to that of SB(−4.10, 2.55, 4.67). Although the physico-geometrical meanings of the kinetic exponents in SB(−4.10, 2.55, 4.67) are difficult to evaluate in the present case, the comparable good fitting by SB(−4.10, 2.55, 4.67) and JMA(3.34) supports the validity of JMA(3.34) as the appropriate model function for interpreting the phsycio-geometrical characteristics of the process. Ideally, JMA(m) with m = 3 is interpreted as the constant rate nucleation and two-dimensional growth or three-dimensional growth of pre-existing nuclei [72,73]. From the morphological observation of three-dimensional growth of rhombohedral particles of calcite, three-dimensional growth of pre-existing nuclei seems to be dominant in the present case. Several causes suggest themselves to explain the deviation of the evaluated m value in JMA(m) from 3. Because of the dendritic branching structure, the reactant is not distributing homogeneously in the space of product growth, resulting in a size-distribution of the calcite particles. This situation is not considered in the ideal nucleation and growth model. Partial involvement of nucleation process in the early stage of the transformation is also expected from the deviations of E_a values from the constant value for the established part of the transformation. The aggregated calcite particles in Fig. 8(b) and the gradual decrease of E_a value in the final stage may suggest the participation of sintering process.

Table 1 summarizes the kinetic results for the thermally induced phase transition from vaterite (ET75AQ25) to calcite. The present kinetic results indicate clearly that the physico-geometric kinetics of the structural phase transition of vaterite to calcite and the morphology and particle size of the product calcite are largely influenced by the morphological characteristics of the reactant vaterite. The findings imply the possibility of further systematic control of calcite in views of the particle morphology and the reactivity by combining the controlled precipitation of CCPs and the thermally induced transformations of those precipitates in the solid-state, because the solid-state transformations can also be controlled by the reaction conditions [37–54].

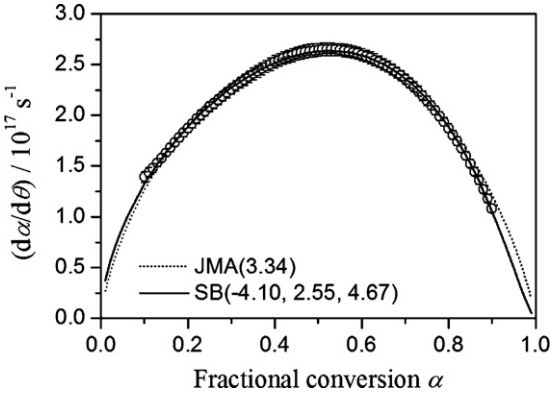

Fig. 12. Comparisons of the experimental master plot of dα/dθ against α with theoretical curves of JMA(m) and SB(m, n, p) models.

4. Conclusions

When exposing an ethanol/water solution of $CaCl_2$ to the gases produced by sublimation–decomposition of solid $(NH_4)_2CO_3$ in a closed vessel, precipitation reactions of CCPs including hydrated ACC take place by the dissolutions of the gases, i.e., NH_3, CO_2, and water vapor, into the $CaCl_2$ solution. The precipitates change from gel-like aggregates of hydrated ACC in absolute ethanol solution to rhombohedral calcite in absolute aqueous solution via co-precipitation of vaterite in mixed ethanol/water solutions of $CaCl_2$. Nearly pure vaterite phase is precipitated from the ethanol/water solution with a volume ratio of ethanol to water around 2–3. The morphology of vaterite changes from a spherical aggregates of nanoparticles to dendrites with increasing the content % of water in the mother liquor. The above findings can be utilized for the selective synthesis of CCPs among the hydrated ACC, vaterite, and calcite and for the morphology control of vaterite from spherical particles to dendrites by the simple method of changing ethanol/water composition of the mother liquor without using organic macromolecule additives.

On heating the series of precipitated samples in an inert gas, several thermally induced transformations characteristic of the component phases in the respective samples are observed. Thermal dehydration of gel water of the hydrated ACC initiates from room temperature, followed by the crystallization of as-produced anhydrous ACC to calcite at the end of the dehydration process, i.e., 500–550 K. Structural phase transition of vaterite to calcite takes place at 750–800 K. All the calcite phases, precipitated from mother solutions and transformed from hydrated ACC or vaterite, decompose quantitatively to CaO at higher than 900 K. The mass-loss traces for the thermal decomposition of calcite in the series of samples are similar in shape except for that of the hydrated ACC precipitated from the absolute ethanol solution and shift systematically to higher temperatures with increasing the water content in the mother liquors due to the increase in the particle size of calcite to be decomposed. Accordingly, it is expected that the present method of precipitation control of CCPs is also useful to control the particle size of calcite produced during heating the precipitated CCPS and to regulate reaction kinetics of ceramic processing including the thermal decomposition of calcite.

The structural phase transition of nearly pure vaterite phase, precipitated from the ethanol/water solution of ET75AQ25 to calcite takes place with $\Delta H = -2.8 \pm 0.1$ kJ mol^{-1}, where rhombohedral particles of calcite grow on the dendrite substrates of vaterite. From the viewpoint of overall kinetics, the established part of the transformation is characterized by the nucleation and growth type model, JMA(3.34), with the apparent value of E_a = 289.9 ± 5.8 kJ mol^{-1}, where the participations of nucleation process and sintering of product particles were expected at the initial and final part of the transformation, respectively. The deviation of the kinetic exponent m = 3.34 in JMA(m) model from the growth dimension 3 was explained by the limitation of the growth size of product calcite by the spatial distribution of the reactant substrates.

Acknowledgment

The present work was supported partially by a grant-in-aid for scientific research (B) (21360340 and 22300272) from Japan Society for the Promotion of Science.

References

[1] S. Mann, Biomineralization: Principles and Concepts in Bioinorganic Materials Chemistry, Oxford University Press, Oxford, 2001.
[2] E. Baeuerlein (Ed.), Biomineralization: Progress in Biology, Molecular Biology and Application", second ed., Wiley-VHC, Weinheim, 2005.
[3] S. Raz, S. Weiner, L. Addadi, Adv. Mater. 12 (2000) 38.
[4] Y. Levi-Kalisman, S. Raz, S. Weiner, L. Addadi, I. Sagi, Adv. Funct. Mater. 12 (2002) 43.
[5] J. Aizenberg, G. Lambert, S. Weiner, L. Addadi, J. Am. Chem. Soc. 124 (2002) 32.
[6] S. Raz, O. Testeniere, A. Hecker, S. Weiner, G. Luquet, Biol. Bull. 203 (2002) 269.
[7] I.M. Weiss, N. Tuross, L. Assadi, S. Weiner, J. Exp. Zool. 293 (2002) 478.
[8] S. Raz, P.C. Hamilton, F.H. Wilt, S. Weiner, L. Addadi, Adv. Funct. Mater. 13 (2003) 480.
[9] L. Addadi, S. Raz, S. Weiner, Adv. Mater. 15 (2003) 959.
[10] Y. Politi, T. Arad, E. Klein, S. Weiner, L. Addadi, Science 306 (2004) 1161.
[11] J.W. Morse, R.S. Arvidson, A. Luttge, Chem. Rev. 107 (2007) 324.
[12] F.C. Meldrum, H. Colfen, Chem. Rev. 108 (2008) 4332.
[13] N.A.J.M. Sommerdijk, G. de With, Chem. Rev. 108 (2008) 4499.
[14] L.B. Gower, Chem. Rev. 108 (2008) 4551.
[15] M. Li, S. Mann, Adv. Funct. Mater. 12 (2002) 773.
[16] L. Xiang, Y. Xiang, Y. Wen, F. Wei, Mater. Lett. 58 (2004) 959.
[17] B. Guillemet, M. Faatz, F. Grohn, G. Wegner, Y. Gnanou, Langmuir 22 (2006) 1875.
[18] C. Wang, J. Zhao, X. Zhao, H. Bala, Z. Wang, Powder Technol. 163 (2006) 134.
[19] T. Kato, Adv. Mater. 12 (2000) 1543.
[20] T. Kato, A. Sugawara, N. Hosoda, Adv. Mater. 14 (2002) 869.
[21] K. Gorna, R. Munoz-Espi, F. Grohn, G. Wegner, Macromol. Biosci. 7 (2007) 163.
[22] L.B. Gower, D.J. Odom, J. Cryst. Growth 210 (2000) 719.
[23] X. Xu, J.T. Han, K. Cho, Chem. Mater. 16 (2004) 1740.
[24] J.T. Han, X. Xu, D.H. Kim, K. Cho, Chem. Mater. 17 (2005) 136.
[25] X. Xu, J.T. Han, K. Cho, Langmuir 21 (2005) 4801.
[26] X. Xu, J.T. Han, D.H. Kim, K. Cho, J. Phys. Chem. B 110 (2006) 2764.
[27] J.R.I. Lee, T.Y.-J. Han, T.M. Willey, D. Wang, R.W. Meulenberg, J. Nilsson, P.M. Dove, L.J. Terminello, T. van Buuren, J.J. de Yoreo, J. Am. Chem. Soc. 129 (2007) 10370.
[28] K. Naka, Y. Chujo, Chem. Mater. 13 (2001) 3245.
[29] E. Lostea, R.M. Wilson, R. Seshadri, F.C. Meldrum, J. Cryst. Growth 254 (2003) 206.
[30] M. Faatz, F. Grohn, G. Wegner, Mater. Sci. Eng. C 25 (2005) 153.
[31] H.S. Lee, T.H. Ha, K. Kim, Mater. Chem. Phys. 93 (2005) 376.
[32] C. Gunther, A. Beckerb, G. Wolf, M. Epple, Z. Anorg. Allg. Chem. 631 (2005) 2830.
[33] S.-C. Huang, K. Naka, Y. Chujo, Langmuir 23 (2007) 12086.
[34] Y. Politi, D.R. Batchelor, P. Zaslansky, B.F. Chmelka, J.C. Weaver, I. Sagi, S. Weiner, L. Addadi, Chem. Mater. 22 (2010) 161.
[35] F.M. Michel, J. MacDonald, J. Feng, B.L. Phillips, L. Ehm, C. Tarabrella, J.B. Parise, R.J. Reeder, Chem. Mater. 20 (2008) 4720.
[36] N. Koga, Y. Yamane, J. Therm. Anal. Calorim. 94 (2008) 379.
[37] A.G. Turnbull, Geochim. Cosmochim. Acta 37 (1973) 1593.
[38] M.S. Rao, Bull. Chem. Soc. Jpn. 46 (1973) 1414.
[39] P. Davies, D. Dollimore, G.R. Heal, J. Therm. Anal. 13 (1978) 473.
[40] C. Barriga, J. Morales, J.L. Tirado, Thermochim. Acta 92 (1985) 211.
[41] C. Barriga, J. Morales, J.L. Tirado, J. Mater. Sci. 21 (1986) 947.
[42] M. Maciejewski, H.-R. Oswald, A. Reller, Thermochim. Acta 234 (1994) 315.
[43] G. Wolf, J. Lerchner, H. Schmidt, H. Gamsjager, E. Konigsberger, P. Schmidt, J. Therm. Anal. 46 (1996) 353.
[44] J. Peric, M. Vucak, R. Krstulovic, L. Brecevic, D. Kralj, Thermochim. Acta 277 (1996) 175.
[45] F. Baitalow, G. Wolf, H.-G. Schmidt, J. Therm. Anal. 52 (1998) 5.
[46] N. Koga, Y. Nakagoe, H. Tanaka, Thermochim. Acta 318 (1998) 239.
[47] G. Wolf, C. Gunther, J. Therm. Anal. Calorim. 65 (2001) 687.
[48] N. Nassrallah-Aboukaïs, J. Jacquemin, C. Decarne, E. Abi-Aad, J.F. Lamonier, A. Aboukais, J. Therm. Anal. Calorim. 74 (2003) 21.
[49] A.W. Searcy, D. Beruto, J. Phys. Chem. 80 (1976) 425.
[50] A.W. Searcy, D. Beruto, J. Phys. Chem. 82 (1978) 163.
[51] M. Maciejewski, A. Reller, Thermochim. Acta 110 (1987) 145.
[52] M. Reading, D. Dollimore, R. Whitehead, J. Therm. Anal. 37 (1991) 2165.
[53] J.M. Criado, M. Gonzalez, J. Malek, A. Ortega, Thermochim. Acta 254 (1995) 121.
[54] N. Koga, J.M. Criado, Int. J. Chem. Kinet. 30 (1998) 734.
[55] A.K. Galwey, Thermochim. Acta 355 (2000) 181.
[56] N. Koga, H. Tanaka, Thermochim. Acta 388 (2002) 41.
[57] J. Aizenberg, A.J. Black, G.M. Whitesides, J. Am. Chem. Soc. 121 (1999) 4500.
[58] K.-S. Seo, C. Han, J.-H. Wee, J.-K. Park, J.-W. Ahn, J. Cryst. Growth 276 (2005) 680.
[59] S.-F. Chen, S.-H. Yu, J. Jiang, F. Li, Y. Liu, Chem. Mater. 18 (2006) 115.
[60] S.R. Dickinson, K.M. McGrath, J. Mater. Chem. 13 (2003) 928.
[61] F.A. Andersen, L. Brecevic, Acta Chem. Scand. 45 (1991) 1018.
[62] N. Koga, J.M. Criado, J. Am. Ceram. Soc. 81 (1998) 2901.
[63] H.L. Friedman, J. Polym. Sci. C 6 (1964) 183.
[64] T. Ozawa, J. Therm. Anal. 2 (1970) 301.
[65] T. Ozawa, J. Therm. Anal. 31 (1986) 547.
[66] N. Koga, Thermochim. Acta 258 (1995) 145.
[67] F.J. Gotor, J.M. Criado, J. Malek, N. Koga, J. Phys. Chem. A 104 (2000) 10777.
[68] T. Ozawa, Bull. Chem. Soc. Jpn. 38 (1965) 1881.
[69] T. Ozawa, Thermochim. Acta 100 (1986) 109.
[70] J.M. Criado, J. Malek, A. Ortega, Thermochim. Acta 147 (1989) 377.
[71] J. Malek, Thermochim. Acta 200 (1992) 257.
[72] H. Tanaka, N. Koga, A.K. Galwey, J. Chem. Educ. 72 (1995) 251.
[73] A. Khawam, D.R. Flanagan, J. Phys. Chem. B 110 (2006) 17315.
[74] G.I. Senum, R.T. Yang, J. Therm. Anal. 11 (1977) 445.
[75] J.H. Flynn, Thermochim. Acta 300 (1997) 83.
[76] J. Sestak, G. Berggren, Thermochim. Acta 3 (1971) 1.
[77] J. Sestak, J. Therm. Anal. 36 (1990) 1997.
[78] L.A. Perez-Maqueda, J.M. Criado, P.E. Sanchez-Jimenez, J. Phys. Chem. A 110 (2006) 12456.
[79] N. Koga, T. Kimizu, J. Am. Ceram. Soc. 91 (2008) 4052.
[80] N. Koga, A. Mako, T. Kimizu, Y. Tanaka, Thermochim. Acta 467 (2008) 11.